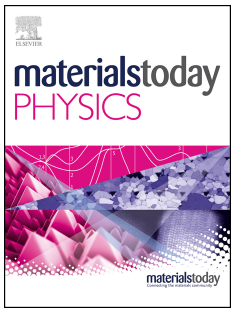

Influence of mechanical motions on the output characteristics of triboelectric nanogenerators

Yang Yu, Qi Gao, Da Zhao, Xiang Li, Zhong Lin Wang, Tinghai Cheng

PII: S2542-5293(22)00099-2

DOI: https://doi.org/10.1016/j.mtphys.2022.100701

Reference: MTPHYS 100701

To appear in: *Materials Today Physics*

Received Date: 29 March 2022

Revised Date: 24 April 2022

Accepted Date: 27 April 2022

Please cite this article as: Y. Yu, Q. Gao, D. Zhao, X. Li, Z.L. Wang, T. Cheng, Influence of mechanical motions on the output characteristics of triboelectric nanogenerators, *Materials Today Physics*, https://doi.org/10.1016/j.mtphys.2022.100701.

CRediT authorship contribution statement

Yang Yu: Conceptualization, Investigation, Writing - Original Draft.
Qi Gao: Investigation, Validation.
Da Zhao: Validation.
Xiang Li: Editing.
Zhong Lin Wang: Conceptualization, Resources, Writing - review & editing, Supervision.
Tinghai Cheng: Conceptualization, Resources, Writing - review & editing, Supervision.

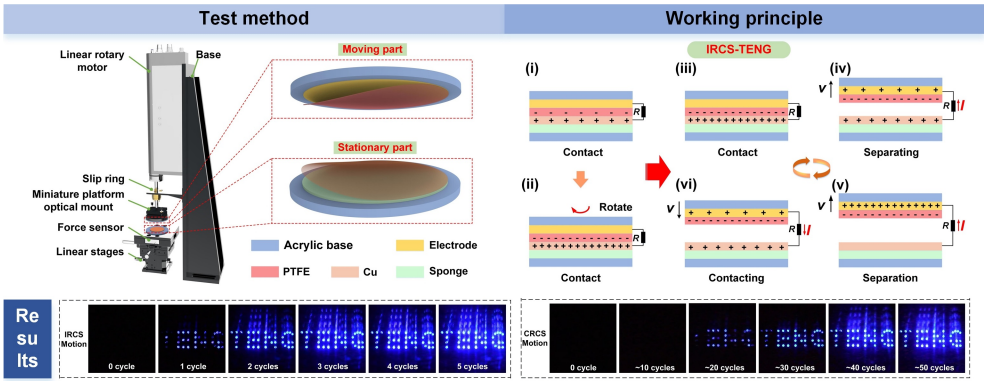

Influence of mechanical motions on the output characteristics of triboelectric nanogenerators

Yang Yu[a, b, 1], Qi Gao[a, b, 1], Da Zhao[a], Xiang Li[a], Zhong Lin Wang[a, b, c, *], Tinghai Cheng[a, b, *]

[a] *Beijing Institute of Nanoenergy and Nanosystems, Chinese Academy of Sciences, Beijing 101400, China*
[b] *School of Nanoscience and Technology, University of Chinese Academy of Sciences, Beijing 100049, China*
[c] *School of Materials Science and Engineering, Georgia Institute of Technology, Atlanta, GA 30332-0245, United States*

[1] *These authors contributed equally to this work.*

*Corresponding authors' e-mail addresses: zhong.wang@mse.gatech.edu, chengtinghai@binn.cas.cn.

Abstract

Triboelectric nanogenerator (TENG) as an energy harvesting device, the output characteristics also affect its applications. Usually, the output characteristics of TENG are considered to be influenced by environmental factors, triboelectric materials, and surface morphology. Here we explore the output characteristics are also influenced by the mechanical motions of friction interfaces for the first time. And two new mechanical motions of TENG are proposed: coupling rotation contact-separation (CRCS) motion and independent rotation contact-separation (IRCS) motion. In addition, the output characteristics of TENG under different mechanical motions are investigated and revealed. It is a universal phenomenon that mechanical motions can affect the output characteristics of TENG verified by different types, different materials, and even different parameters of TENG. Compared with contact-separation (CS) motion, the transferred charges and output power of TENG under CRCS motion and IRCS motion realize 397%, 483% and 440%, 660% enhancement, respectively. Furthermore, the theoretical models describing dynamic charging and discharging under different mechanical motions are established. Finally, it is proved that changing mechanical motions can affect the collection of energy. This study provides a new factor to influence the output characteristics of TENG, which can guide the design and accelerate the practical applications of TENG.

Keywords: mechanical motions, triboelectric nanogenerator, friction interfaces, output characteristics

1. Introduction

The 21st century is an age full of information, intelligence, and automation. Intelligent connect, as a new concept, will be combined with the 5th generation mobile networks (5G), artificial intelligence, and the Internet of Things (IoT) to become a catalyst for accelerating the development of science and technology in the future, and will become a new disruptive technology. In this link, distributed sensors will play an indispensable part in information collection and transmission, which is one of the necessary hardware to realize the IoT [1-6]. Recent research shows that there will be more than 30 billion sensors used for information obtain by 2025 [7]. However, it is a huge challenge to power such a large number of sensors if we rely on conventional batteries, solar cells, etc [8].

In 2012, a new type of power harvesting device, triboelectric nanogenerator

(TENG) is invented by Wang's group [9], the challenge will be greatly improved in the future. TENG is based on coupling contact electrification and electrostatic induction [10-12], which can convert the small micro/nano energy into electrical energy [13, 14], such as wind [15, 16], flowing water [17, 18], vibration [19, 20], human motion [21, 22], walking [23, 24], and mechanical triggering [25, 26]. At the same time, TENG has advantages of low-cost, easy fabrication, abundant materials choice, widely adaptable and environmental friendliness, etc [27-29]. TENG is expected to capture energy from the environment and achieve a stable energy supply for distributed IoT sensors [30]. As an energy harvesting device, the output characteristics also influence the applications of TENG. Therefore, it is very important to explore the factors affecting the output characteristics of TENG, which can guide the design and accelerate the practical applications of TENG. Usually, TENG devices are considered to be influenced by environmental factors, triboelectric materials, and surface morphology. Humidity [31, 32], temperature [33, 34], and pressure of the environment [35, 36] are regarded as the main elements that influence the output characteristics by the environment. Changing the size, contact force, and modifying the surface properties of the triboelectric materials affect the actual contact area and then influence the output characteristics of TENG [37-39]. Recently, the power management (PM) circuits are regarded as another effective method that can increase the charge density [40-42]. Although some influence factors have been explored, it is still necessary to explore other ways affecting the output characteristics of TENG. Nowadays, TENG can be divided into contact-separation mode TENG (CS-TENG), single-electrode mode TENG (SEC-TENG), free-standing mode TENG (FS-TENG), and lateral sliding mode TENG (LS-TENG). And mechanical motions between friction interfaces of the above TENG have only two types: one is only linear motion, the other is only rotary motion as shown in Figure S1. However, whether other mechanical motions can affect the output characteristics of TENG is not clear.

Here, we first demonstrate the mechanical motions of friction interfaces can influence output characteristics of TENG. And two new mechanical motions of friction interfaces for TENG are proposed, one is coupling rotation contact-separation (CRCS) motion and the other is independent rotation contact-separation (IRCS) motion. Furthermore, the Influence of mechanical motions on the output characteristics of TENG are investigated and revealed. And the influence is a universal phenomenon to change the characteristics verified by different types, different materials, and even different parameters (contact force, electrode diameter, rotation speed) of TENG. Experimental results show that with different materials, IRCS motion and CRCS motion promote transferred charges by approximately 2-5 times compared with contact-separation (CS) motion. And the output power of TENG under CRCS motion and IRCS motion realizes 440% and 660% enhancement, respectively. In addition, the mechanical motions on TENG's characteristics are analyzed, and theoretical models of dynamic charging and discharging are established. Finally, it is proved that changing the mechanical motions of TENG also affects the ability to harvest environmental

energy. This work provides a new factor to influence the output characteristics of TENG, and also can expand the field of TENG applications.

2. Results and discussion

2.1 Structure and working mechanism of TENGs

To study the influence of mechanical motions between friction interfaces on the output characteristics of TENGs, a standard solid-solid experimental test system with controllable temperature and humidity is established (Supporting Information, Figure S2). The measurement system can achieve different mechanical motions (Figure 1a, Supporting Information Note S1). The TENG mainly contains a moving part and a stationary part. The moving part consists of an acrylic base, an electrode, and polytetrafluoroethylene (PTFE). The stationary part is composed of an acrylic base, a sponge, and a Cu. The CS-TENG is a typical representative of TENG with contact-separation (CS) motion. The working principle is shown in Fig. 1b. In the initial state, because of differences in Cu and PTFE electronegativity, they generate an equal amount of charge of opposite signs at their contact interfaces [Fig. 1b(i)]. Then they separate, the electrons in the external circuit flow from the electrode to Cu [Fig. 1b(ii)]. When the separation distance reaches L (which is more than 10 times the thickness of the PTFE film d), the charge transferred is almost at a maximum [Fig. 1b(iii)] [43]. Eventually, PTFE gradually approaches Cu, the electrons flow to the electrode [Fig. 1b(iv)]. By cyclically repeating these four phases, the CS-TENG produces a continuous power output.

On the basis of CS-TENG, two new mode TENGs are proposed by changing relative mechanical motions between friction interfaces: one is independent rotation contact-separation mode TENG (IRCS-TENG), and the other is coupling rotation contact-separation mode TENG (CRCS-TENG). IRCS-TENG is achieved by independent rotation contact-separation (IRCS) motion which comprises two phases as shown in Fig. 1c: First, the Cu and PTFE are brought into contact [Fig. 1c(i)] and then rotated through one revolution [Fig. 1c(ii)]. Then, a number of CS motions are performed [Fig. 1c(iii)- Fig. 1c(vi)]. The one revolution is regarded as one operation cycle of the IRCS motion. CRCS-TENG is achieved by coupling rotation contact-separation (CRCS) motion which moves with a straight reciprocating motion while rotating as shown in Fig. 1d. Each contact between the Cu and PTFE is regarded as one operation cycle of the CRCS motion. The working principle of IRCS-TENG and CRCS-TENG is similar to CS-TENG except that they have different transferred charges between Cu and PTFE.

To measure the influence of mechanical motions on the output characteristics, TENG is driven by CS motion, CRCS motion, and IRCS motion is researched. The entire experiment is set at constant temperature and humidity of 20°C and 45% in relative humidity, respectively. The whole system is almost without noise which is presented in Supporting Information, Fig. S3. Comparisons of the transferred charge, short-circuit current, and open-circuit voltage under CS, CRCS and IRCS motions (Fig.

1e-1g). It is obvious that the output characteristics of TENG can be obviously influenced by changing the relative mechanical motions between friction interfaces. Compared with CS motion, the transferred charges of TENG under CRCS motion and IRCS motion increase from 27.2 nC to 53.3 nC and 81.2 nC, promoting by approximately 2.0 and 3.0 times. Furthermore, the short-circuit current and open-circuit voltage have a similar promoting tendency. The short-circuit current and open-circuit voltage increase from 1.4 μA to 2.9 μA and 5.2 μA, and from 65.7 V to 120.6 V and 186.7 V.

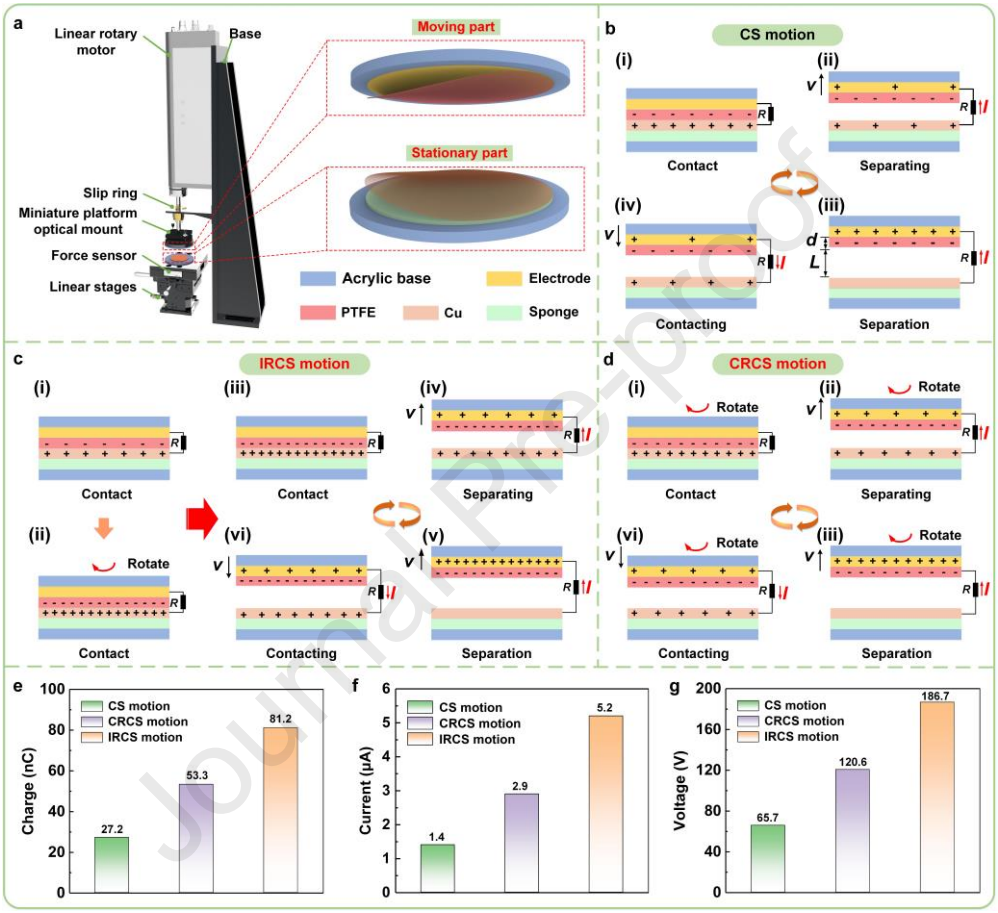

Fig. 1. The structure and working mechanism of TENG. a) Three-dimensional model of measurement system and structure of TENG. b) The working principle of CS-TENG. c) The working principle of IRCS-TENG. d) The working principle of CRCS-TENG. e) Transferred charge, f) short-circuit current, and g) open-circuit voltage comparison between CS-TENG, CRCS-TENG, and IRCS-TENG.

2.2 Output characteristics of TENG under different mechanical motions

The output characteristics of TENG under CRCS motion and IRCS motion are studied. CRCS-TENG is first studied, and the experiment proceeded as follows: we make the motor with linear motion (CS motion) in Fig. S4 and Note S2 and rotary motion (speed of 60 rpm) at the same time. The dynamic charging of CRCS-TENG with the diameter of 60 mm is shown in Fig. 2a. It can be seen that the transferred charge increases rapidly and then slows down. Comparisons of the open-circuit voltage and short-circuit current under CS motion and CRCS motion are presented in Fig. 2b,

c. It shows the short-circuit current, and open-circuit voltage of TENG have been significantly influenced by the CRCS motion.

Then, IRCS-TENG is studied. The experiment proceeded as follows: On the basis of CS motion, the motor first returns to its initial position, which places the two tested materials in contact with a 2 N force. The motor is then set to rotate 1 revolution clockwise with a speed of 60 rpm. Then PTFE moves with CS motion. At this time, the transferred charge is that of IRCS-TENG after a single operation cycle. Continuous measurements of the transferred charge after 2, 3, 4, and 5 operation cycles are tested using the same method. Fig. 2d shows that, in the first three operation cycles, the transferred charges under IRCS motion increase rapidly. For the fourth and fifth operation cycles, the transferred charge gradually approaches a certain saturation value. The open-circuit voltage and short-circuit current under IRCS motions (Fig. 2e, f) exhibit increasing trends that are similar to the transferred charge. Moreover, the charge retention characteristics after five operation cycles of the IRCS motion (Fig. 2g) are researched. And the amount of the transferred charges with CS motion begins to decay rapidly and then gradually stabilizes. Enlarged views for specific time intervals are presented in Fig. 2h. After approximately 100,000 cycles (30 hours), the transferred charge is almost stable with 64.8 nC, which is approximately 2.4 times that under the initial CS motion. This means that the transferred charge added by changing mechanical motions can remain at the friction interfaces for a long time.

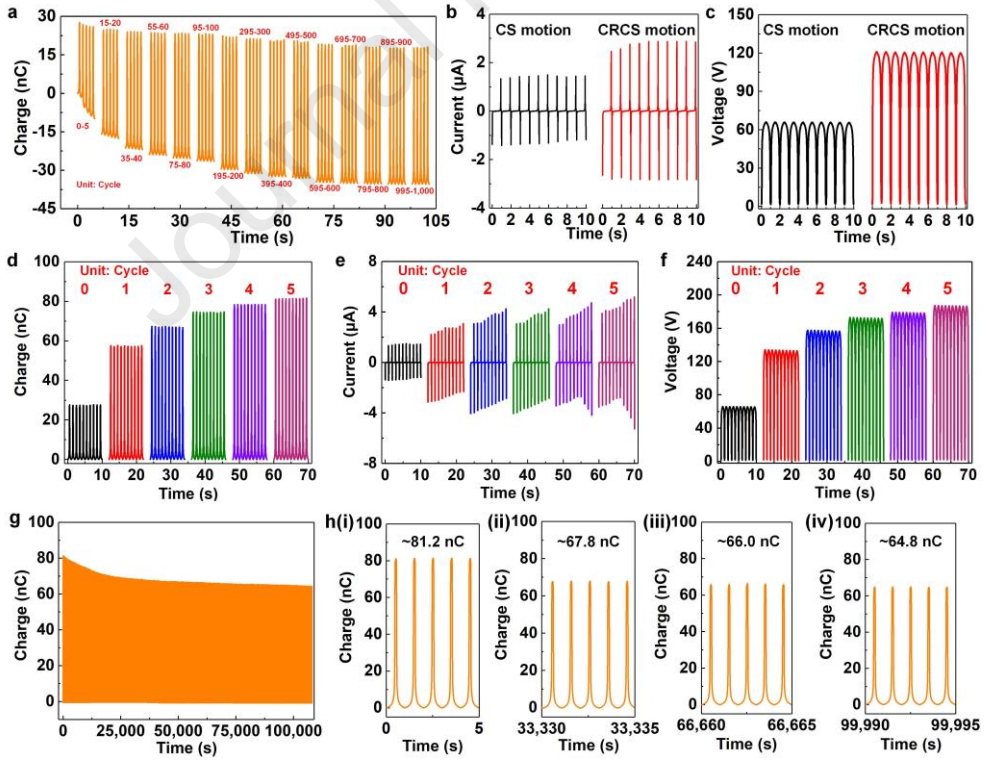

Fig. 2. Output characteristics of TENG under different mechanical motions. a) Transferred charge of CRCS-TENG. b, c) Comparison of short-circuit current and open-circuit voltage between CS-TENG and CRCS-TENG. d-f) Transferred charge, short-circuit current, and open-circuit voltage of

IRCS-TENG. g, h) Charge retention characteristic after IRCS motion and enlarged views for specified time intervals.

2.3 Universality of influence of mechanical motions on TENG's output characteristics

To prove that the influence of mechanical motions on TENG's output characteristics is a universal phenomenon. The influences of mechanical motions on the transferred charge with different parameters are firstly studied. The results show an improvement rate of transferred charge under different contact force, electrode diameters, and rotation speeds under CRCS motion and IRCS motion are all more than 1 as shown in Fig. 3a-3c and 3d-3f, respectively. And the dynamic charging processes are shown in the Supporting Information Fig. S5-S10. It shows that CRCS motion and IRCS motion are effective in affecting the output characteristics with materials Cu and PTFE even with different parameters. It can be seen that larger contact force, smaller electrode diameters are more conducive for CRCS motion and IRCS motion to improve the charge transferred. This is because larger contact force and smaller electrode diameters make the Cu film and PTFE film contact fully. Furthermore, for CRCS motion, the higher the rotation speed is, the more effective the improvement rate of transferred charge is. This is because higher speeds increase the angle of friction between the two materials during contact. However, with the higher rotation speed, the improvement rate of transferred charge by IRCS motion is slightly reduced. This may be if the speed is too high, the interfaces of Cu and PTFE will contact inadequacy.

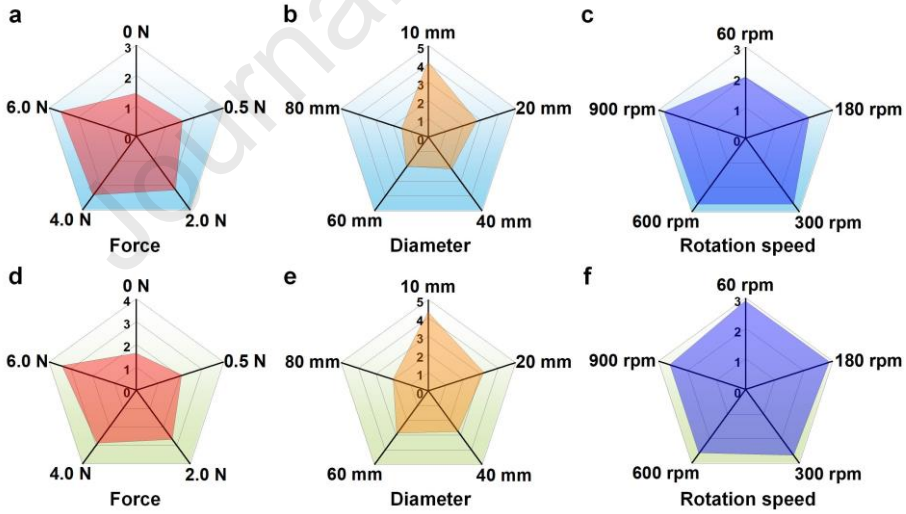

Fig. 3. The improvement rate of transferred charge by CRCS motion and IRCS motion: a-c) and d-f) are the improvement rates of transferred charge by CRCS motion and IRCS motion under different contact force, electrode diameters, and rotation speeds.

Then, the output characteristics of TENG with other materials are also compared to further verify the influence of different mechanical motions on TENG's output characteristics is universal. The comparison of the transferred charges with other materials Cu-Kapton, Al-PTFE, Al-Kapton, and Nylon-PTFE are shown in Fig. 4a, 4d, 4g, and 4j, respectively. And the dynamic charging processes are shown in the

Supporting Information Fig. S11-S12. The transferred charges of CRCS-TENG with different materials (Cu-Kapton, Al-PTFE, Al-Kapton, and Nylon-PTFE) are 62.9 nC, 48.9 nC, 44.9 nC, and 63.2 nC, promotes by approximately 342%, 217%, 397%, and 165% compared with CS-TENG. IRCS-TENG is more conducive to transferred charge enhancement which promotes by approximately 420%, 337%, 483%, and 218% compared with CS-TENG. The short-circuit current and open-circuit voltage of CRCS-TENG and IRCS-TENG exhibit a similar increasing tendency (Figure 4b-4c, 4e-4f, 4h-4i, 4k-4l). The experimental results show that the output characteristics of TENG are greatly influenced by changing the mechanical motions with different materials. Additionally, the output characteristics of traditional SE-TENG with different mechanical motions are also studied as shown in Supporting Information Fig. S13. It shows the CRCS motion and IRCS motion can also influence the output characteristics of SE-TENG. These results demonstrate that it is a universality phenomenon that changing mechanical motions can influence the output characteristics of TENGs.

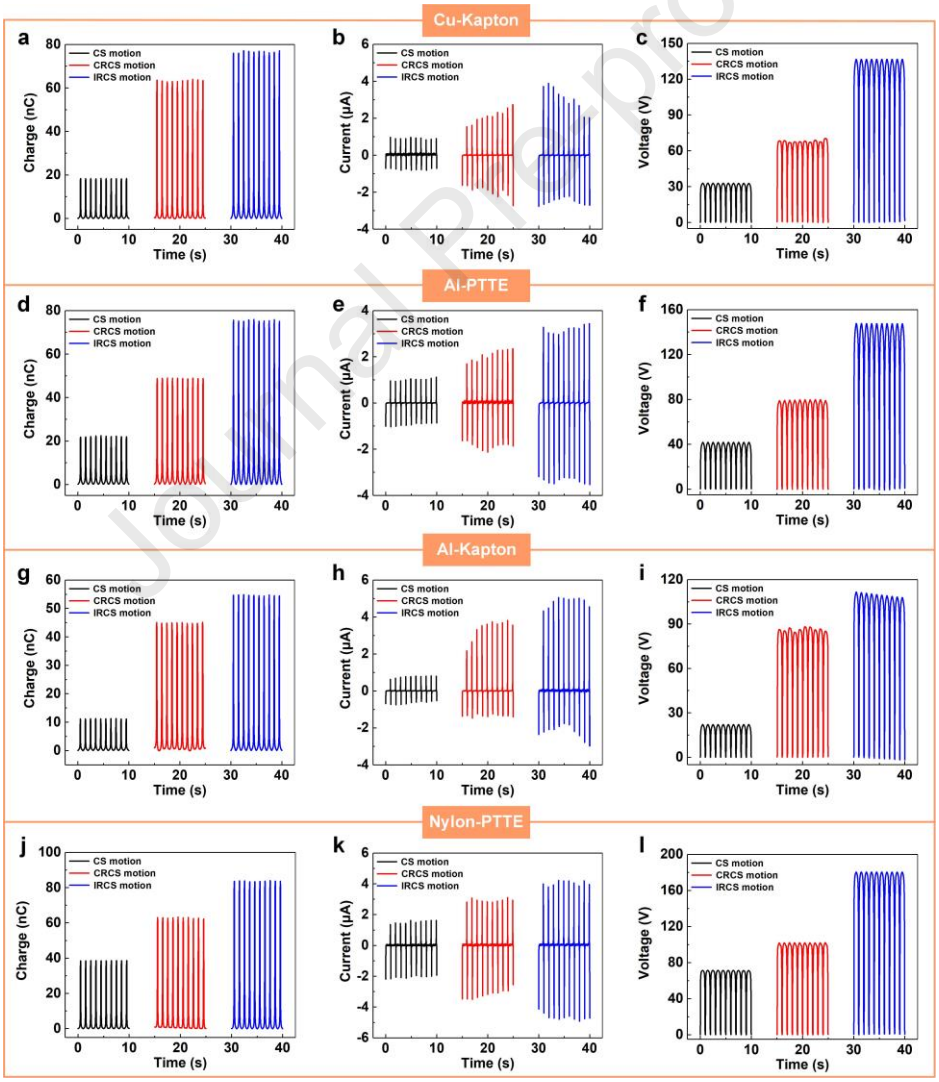

Fig. 4. The output performance of CS-TENG, CRCS-TENG, and IRCS-TENG with different materials. a-c) Transferred charge, short-circuit current, and open-circuit voltage with Cu-Kapton. d-f) Transferred charge, short-circuit current, and open-circuit voltage with Al-PTFE. g-i)

Transferred charge, short-circuit current, and open-circuit voltage with Al-Kapton. j-l) Transferred charge, short-circuit current, and open-circuit voltage with Nylon-PTFE.

2.4 Mechanism of influence of mechanical motions on TENG's output characteristics

For practical TENG devices, tested materials are not completely flat, there would be a lot of air voids existence when they contact as shown in Fig. 5a. And electron transfer occurs mainly in the areas which the tested materials actually contact. The electron at the non-contact area cloud not overlap on the non-contact interfaces as shown in Fig. 5b. As a result, the total number of transferred charges is limited to the actual contact area of the tested materials. When TENG devices driven by CRCS motion and IRCS motion, the contact phase will be a dynamic sweeping process, and non-contact areas may become closer or come into contact such as areas A and B. Which increases actual contact areas (electron cloud overlap on the contact areas as shown Fig. 5c) and thus enhances triboelectrification (TE). So the TENG devices have higher output performance under CRCS motion and IRCS motion than traditional TENG devices. To further explain the mechanisms of the mechanical motions that influence the output characteristics of TENG. Here, considering the inadequacy of contact in TENG, which is the actual contact area is less than the electrode area. We define a contact efficiency as:

$$\eta = \frac{S'}{S}, \tag{1}$$

where S' is the actual area, the S is the electrode area. The charge density can be calculated as follows:

$$\sigma = \frac{Q}{S} = \frac{\sigma' S'}{S} = \sigma' \eta, \tag{2}$$

where Q is the transferred charges of TENG and σ' is the charge density of the contact area. So the charge density of TENG under different mechanical motions can be described as follows:

$$\sigma_{CS} = \sigma' \eta_{CS}, \tag{3}$$

$$\sigma_{CRCS} = \sigma' \eta_{CRCS}, \tag{4}$$

$$\sigma_{IRCS} = \sigma' \eta_{IRCS}, \tag{5}$$

the σ_{CS}, σ_{CRCS}, σ_{IRCS} and η_{CS}, η_{CRCS}, η_{IRCS} are the charge density and contact efficiency of CS-TENG, CRCS-TENG, and IRCS-TENG, respectively. Due to their motion characteristics, for the CRCS-TENG, tested materials rotate relative to each other only at the moment when they contact, and the relative rotation angle is less than 360°. For the IRCS-TENG, the tested material keep in contact with each other during the process of relative rotation, and the relative rotation angle is 360° as shown in Supporting Information, Fig. S14. So $\eta_{CS}<\eta_{CRCS}<\eta_{IRCS}$, $\sigma_{CS}<\sigma_{CRCS}<\sigma_{IRCS}$. And the output characteristics of CS-TENG, CRCS-TENG, and IRCS-TENG gradually increase. Simulation of electrical potential distributions shows the electrical potential under CS motion, CRCS motion, and IRCS motion also gradually increases which is the same as the above experiments and analysis (Supporting Information, Fig. S15).

In order to better reveal the dynamic influence of mechanical motions on the transfer charge of TENG, the relationship between the charge improving rate q_n and number of the working cycle under CRCS motion and IRCS motion with different materials are shown in Fig. 5d and 5e, respectively. The improving rate q_n is defined as:

$$q_n = \frac{Q_n}{Q_0}, \tag{6}$$

where Q_0 denotes the transferred charges under CS motion, and similarly Q_n denotes the transferred charges when operating for n cycles under IRCS motion or CRCS motion. The experimental results show that the Q_n increases rapidly at first and then gradually approaches a certain saturation value which satisfies the law of exponential growth. According to the model for charging an insulating sphere rolling on a plane metal surface [44], theoretical model for dynamic charging under CRCS motion and IRCS motion (Supporting Information, Notes S3) is established. For the charging process, Q_n is calculated from:

$$Q_n = -Q_s e^{-n/\tau} + (Q_0 + Q_s), \tag{7}$$

where n indexes the operation cycle, Q_s denotes the maximum charge accumulation under IRCS motion or CRCS motion, Q_0 is the charge transferred under CS motion and τ is the time constant for charging. Subsequently, q_n for the charging process can be calculated:

$$q_n = a e^{-n/\tau} + b, \tag{8}$$

where $a = -\frac{Q_s}{Q_0}$ and $b = \frac{Q_0 + Q_s}{Q_0}$.

The curves obtained from the theoretical model are compared with experimental data to verify the correctness in modeling charging (Figure 5d and 5e). The theoretical results are in agreement with the experimental results. The fitting values of the parameters corresponding to CRCS motion and IRCS motion are listed in Supporting Information, Tables S2 and S3.

Moreover, the charge retention characteristics (discharging) of the IRCS motion are studied with the same method (Supporting Information, Notes S3). The model for discharging process, q_n can be expressed as:

$$q_n = c e^{-\beta n}, \tag{9}$$

where $c = \frac{Q_n}{Q_0}$, and β denotes a constant that represents the unit rate of discharge. Similarly, the results obtained from the theoretical model for dynamic discharge are compared with the experimental results (Fig. 5f). The fitting values for the parameters are listed in Supporting Information, Table S4. The above theoretical model provides an important theoretical basis for a better understanding and practical applications of mechanical motions affecting the performance of TENG.

And the surface topography of each material is studied, specifically the surface roughness (Fig. 5g). The 3D images of the dielectric surfaces of Kapton, PTFE, Al, Cu, and Nylon are shown in Fig. 5h-5l. The test results show that Kapton has a smoother surface than PTFE. In other words, Kapton film makes more contact with other materials than PTFE film and the dynamic charging process becomes more complete

[45]. This may be the reason why the output performance with Kapton increased higher than that of PTFE in the above experiment.

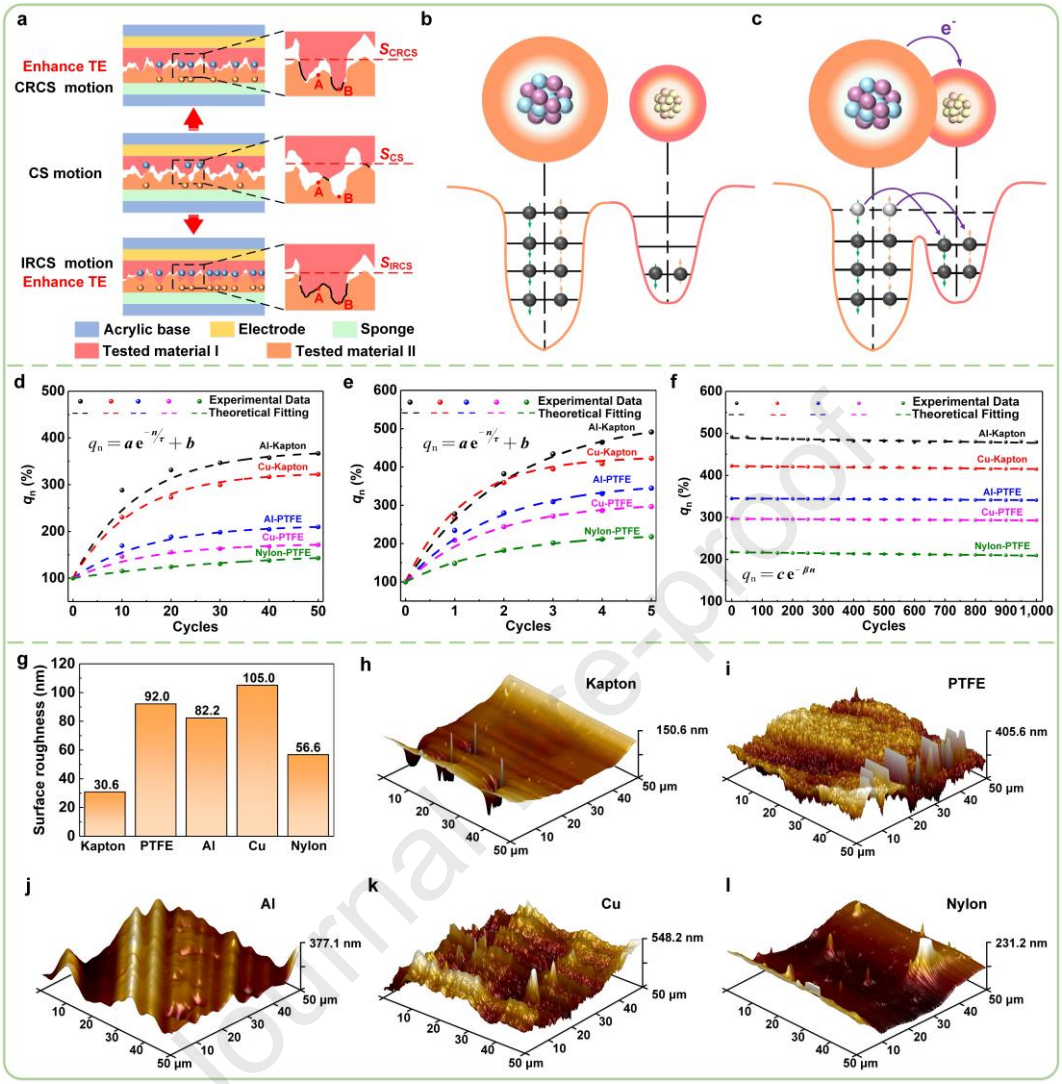

Fig. 5. The working mechanism of mechanical motions for influencing the characteristics of TENG. a) Working mechanism of influencing the performance of TENG by mechanical motions. b, c) Electron-cloud-potential-well model depicting the charge transfer between two tested materials non-contact and after contact [46]. Comparisons of curves calculated using the theoretical model for charging and obtained from experimental results under d) CRCS motion and e) IRCS motion. f) A similar comparison for discharging after IRCS motion. g) Histogram of the surface roughness of materials used. h-l) 3D images of the dielectric surface of different materials.

2.5 Application of TENG with different mechanical motions

To further demonstrate that mechanical motions between friction interfaces can influence the output characteristics of TENG and facilitate its application. The charge curves of various capacitors for voltages up to 1.5 V under different mechanical motions with materials of Al-Kapton are firstly studied as shown in Fig. 6a-6c. The experimental results show that the charging time of the capacitor is obviously different from the different mechanical motions. Charging rates by CRCS motion and IRCS motion are approximately 2 and 3 times higher than that by CS motion. Which indicates

higher output performance of CRCS motion and IRCS motion than that of CS motion. In addition, the charge curves of various capacitors with materials of Nylon-PTFE are also studied which shows the same regular (Supporting Information, Fig. S16a-S16c).

Next, the open-circuit voltage, short-circuit current, and peak power are also measured under various external loads with materials Al-Kapton as shown in Fig. 6d-6f. It shows that the open-circuit voltage and short-circuit current have been enhanced by CRCS motion and IRCS motion under various external loads compared with CS motion. Furthermore, compared with CRCS motion and IRCS motion, the maximum power of the TENG increase from 3.5 μW to 15.9 μW and 23.1 μW, promoting by approximately 440% and 660% times. And materials of Nylon-PTFE are also reached which shows the same regular (Supporting Information, Fig. S16(d)-S16(f)).

Finally, the capability to power an array of LED lights under CS motion, CRCS motion, and IRCS motion with the Al and Kapton materials is studied (Supporting Information, Movies S1 and S2). As depicted in Fig. 6g, under CS motion (0 cycle), the LED lights can not be lit up. However, under CRCS motion and IRCS motion, the LEDs light up gradually as the operating cycle increases. When under the IRCS motion, with 1-3 operation cycles, the LED lights gradually light up, and for 4 and 5 operation cycles, the brightness of all the LED lights are almost the same. When under CRCS motion, with 20 operation cycles, the LED lights gradually light up. The brightness of all the LED lights are nearly the same for 40-50 operation cycles. These results further illustrate that the characteristics of TENG can be influenced by mechanical motions.

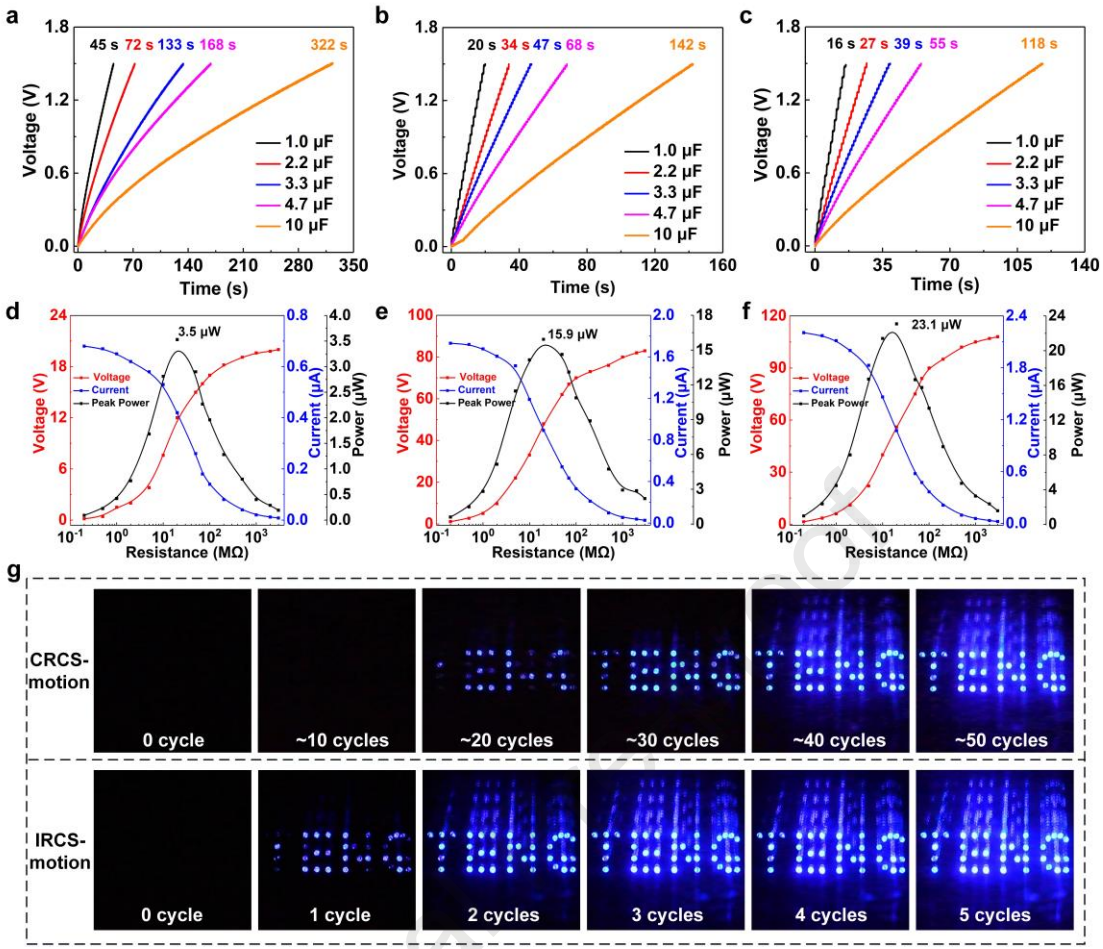

Fig. 6. Output characteristics and application with Al-Kapton under different mechanical motions with Al-Kapton: Charging capacity for different capacitors under a) CS motion, b) CRCS motion, and c) IRCS motion. Load voltage, load current and the peak power under d) CS motion, e) CRCS motion, and f) IRCS motion. g) Performance comparison of video snapshots under IRCS motion and CRCS motion.

3. Conclusions

In this work, the mechanical motions can influence the output characteristics of TENGs was first demonstrated. Two new mechanical motions of TENG were proposed, one is CRCS motion and the other is IRCS motion. And the output characteristics of TENG under different mechanical motions are investigated. According to the comparison experiments for different types, different materials, and even different parameters of TENG, the universality of the mechanical motions affecting the output characteristics of TENG was verified. IRCS motion and CRCS motion with different materials promoted charge transfers by approximately 2-5 times compared with traditional CS motion. With the material Al and Kapton, the charge transfers and output power under CRCS motion and IRCS motion realize 397%, 483%, and 440%, 660% enhancement, respectively. Besides, the mechanism of mechanical motions on TENG's characteristics is revealed. And theoretical models describing dynamic charging and discharging of TENG under CRCS motion and IRCS motion are proposed and

established. Finally, it is proved that mechanical motions have the ability to affect the collection of environmental energy. This work provides a new and simple factor to change the output characteristics of TENG, which is beneficial to promote the applications of TENG in energy harvesting.

4. Experimental section

Fabrication of the TENG: Two acrylic plates of thickness 3 mm are cut into disks of diameter 100 mm using a carbon dioxide laser cutting machine (31 Degree 6090). For one part, Cu foils of different dimensions (10 mm, 20 mm, 40 mm, 60 mm, and 80 mm) are added to form electrodes on the acrylic plates. One Tested material is pasted onto the Cu foils. For the other part, sponges of matching dimensions as the foils (10 mm, 20 mm, 40 mm, 60 mm, and 80 mm) with a thickness of 1 mm are added to the different acrylic plates. The other tested materials of the same dimensions as the sponge were pasted onto the sponge. If the material is nylon, a Cu foil should be added below it as an electrode.

Measurements: A constant temperature and humidity test chamber (Y-HF-960L, Yuhang Zhida, China) is used to adjust temperature and humidity. A linear rotary motor (PR-52, LinMot, Switzerland) provided the external impulses. The linear stages consist of a lifting platform (AKV10A-90C, Zolix, China), an adapter plate (BP-A100, Zolix, China), and two horizontal platforms (AK25A-10020C, AK25A-10020CZ, Zolix, China) that adjusted the contact force and coaxiality between the two tested materials. The contact force was measured directly using a force sensor (ZZ-420, Zhizhan Measurement&Control, China). A miniature platform optical mount (Npmv50, Zolix, China) adjusted the horizontal level of the tested material. The surface topography of the materials is tested using an atomic force microscope (icon, Bruker, Germany). The transferred charge, open-circuit voltage, and short-circuit current were measured using an electrometer (6514, Keithley, USA). All measurements were recorded using a data acquisition system (USB-6218, National Instruments, USA) and stored using the program LabVIEW.

Declaration of competing interest

We declare that we do not have any commercial or associative interest that represents a conflict of interest in connection with the work submitted.

Acknowledgments

The authors are grateful for the support from the Beijing Natural Science Foundation (No. 3222023), and the National Key R & D Project from the Minister of Science and Technology (Nos. 2021YFA1201601 and 2021YFA1201604).

Data availability

The data that support the findings of this study are available from the corresponding authors upon reasonable request.

Credit author statement

Yang Yu: Conceptualization, Investigation, Writing - Original Draft. Qi Gao: Investigation, Validation. Da Zhao: Validation. Xiang Li: Editing. Zhong Lin Wang: Conceptualization, Resources, Writing - review & editing, Supervision. Tinghai Cheng: Conceptualization, Resources, Writing - review & editing, Supervision.

References

[1] W. Liu, Z. Wang, C. Hu, Advanced designs for output improvement of triboelectric nanogenerator system, Mater. Today 45 (2021) 93-119, https://doi.org/10.1016/j.mattod.2020.11.012.

[2] Q. Shi, B. Dong, T. He, Z. Sun, J. Zhu, Z. Zhang, et al., Progress in wearable electronics/photonics—Moving toward the era of artificial intelligence and internet of things, InfoMat 2 (2020) 1131-62, https://doi.org/10.1002/inf2.12122.

[3] M. Zhu, Z. Yi, B. Yang, C. Lee, Making use of nanoenergy from human – Nanogenerator and self-powered sensor enabled sustainable wireless IoT sensory systems, Nano Today, 36 (2021) 101016, https://doi.org/10.1016/j.nantod.2020.101016.

[4] L. Liu, Q. Shi, C. Lee, A novel hybridized blue energy harvester aiming at all-weather IoT applications, Nano Energy, 76 (2020) 105052, https://doi.org/10.1016/j.nanoen.2020.105052.

[5] L. Liu, X. Guo, C. Lee, Promoting smart cities into the 5G era with multi-field Internet of Things (IoT) applications powered with advanced mechanical energy harvesters, Nano Energy, 88 (2021) 106304, https://doi.org/10.1016/j.nanoen.2021.106304.

[6] Z. Sun, M. Zhu, C. Lee, Progress in the Triboelectric Human–Machine Interfaces (HMIs)-Moving from Smart Gloves to AI/Haptic Enabled HMI in the 5G/IoT Era, Nanoenergy Advances, 1 (2021) 81-121, https://doi.org/10.3390/nanoenergyadv1010005.

[7] Z.L. Wang, Entropy theory of distributed energy for internet of things, Nano Energy 58 (2019) 669-72, https://doi.org/10.1016/j.nanoen.2019.02.012.

[8] H. Liu, J. Zhong, C. Lee, S.-W. Lee, L. Lin, A comprehensive review on piezoelectric energy harvesting technology: Materials, mechanisms, and applications, Appl. Phys. Rev 5 (2018) 041306, https://doi.org/10.1063/1.5074184.

[9] F.-R. Fan, Z.-Q. Tian, Z. Lin Wang, Flexible triboelectric generator, Nano Energy 1 (2012) 328-334, https://doi.org/10.1016/j.nanoen.2012.01.004.

[10] Z.L. Wang, From contact electrification to triboelectric nanogenerators, Rep. Prog. Phys. 84 (2021), 096502, https://pubmed.ncbi.nlm.nih.gov/34111846/.

[11] Z.L. Wang, On Maxwell's displacement current for energy and sensors: the origin of nanogenerators, Mater. Today 20 (2017) 74-82, https://doi.org/10.1016/j.mattod.2016.12.001.

[12] J. Shao, T. Jiang, Z. Wang, Theoretical foundations of triboelectric nanogenerators (TENGs), Sci. China: Technol. Sci. 63 (2020) 1087-109, https://doi.org/0.1007/s11431-020-1604-9.

[13] C. Zhang, W. Tang, C. Han, F. Fan, Z.L. Wang, Theoretical comparison, equivalent transformation, and conjunction operations of electromagnetic induction generator and triboelectric nanogenerator for harvesting mechanical energy, Adv. Mater. 26 (2014) 3580-3591, https://doi.org/10.1002/adma.201400207.

[14] Q. Zheng, B. Shi, F. Fan, X. Wang, L. Yan, W. Yuan, et al., In vivo powering of pacemaker by breathing-driven implanted triboelectric nanogenerator, Adv. Mater. 26 (2014) 5851-5856, https://doi.org/10.1002/adma.201402064.

[15] L. Zhang, B. Zhang, J. Chen, L. Jin, W. Deng, J. Tang, et al., Lawn structured triboelectric nanogenerators for scavenging sweeping wind energy on rooftops, Adv. Mater. 28 (2016) 1650-1656, https://doi.org/10.1002/adma.201504462.

[16] T. Cheng, Y. Li, Y.-C. Wang, Q. Gao, T. Ma, Z.L. Wang, Triboelectric nanogenerator by integrating a cam and a movable frame for ambient mechanical energy harvesting, Nano Energy 60 (2019) 137-43, https://doi.org/10.1016/j.nanoen.2019.03.019.

[17] Y. Wang, Z. Wang, D. Zhao, X. Yu, T. Cheng, G. Bao, et al., Flow and level sensing by waveform coupled liquid-solid contact-electrification, Mater. Today Phys. 18 (2021) 100372, https://doi.org/10.1016/j.mtphys.2021.100372.

[18] M. Yin, X. Lu, G. Qiao, Y. Xu, Y. Wang, T. Cheng, et al., Mechanical regulation triboelectric nanogenerator with controllable output performance for random energy harvesting, Adv. Energy Mater. 10 (2020) 2000627, https://doi.org/10.1002/aenm.202000627.

[19] E.M. Wardhana, H. Mutsuda, Y. Tanaka, T. Nakashima, T. Kanehira, N. Taniguchi, et al., Harvesting contact-separation-compression vibrations using a flexible and compressible triboelectric generator, Sustain. Energy Technol. Assess. 42 (2020) 100869, https://doi.org/10.1016/j.seta.2020.100869.

[20] M.A. Adly, M.H. Arafa, H.A. Hegazi, Modeling and optimization of an inertial triboelectric motion sensor, Nano Energy 85 (2021) 105952, https://doi.org/10.1016/j.nanoen.2021.105952.

[21] K. Dong, J. Deng, Y. Zi, Y.C. Wang, C. Xu, H. Zou, et al., 3D orthogonal woven triboelectric nanogenerator for effective biomechanical energy harvesting and as self-powered active motion sensors, Adv. Mater. 29 (2017) 1702648, https://doi.org/10.1002/adma.201702648.

[22] X. Pu, L. Li, M. Liu, C. Jiang, C. Du, Z. Zhao, et al., Wearable self-charging power textile based on flexible yarn supercapacitors and fabric nanogenerators, Adv. Mater. 28(2016) 98-105, https://doi.org/10.1002/adma.201504403.

[23] C. Deng, W. Tang, L. Liu, B. Chen, M. Li, Z.L. Wang, Self -powered insole plantar pressure mapping system, Adv. Funct. Mater. 28 (2018) 1801606, https://doi.org/10.1002/adfm.201801606.

[24] Z. Lin, Z. Wu, B. Zhang, Y.-C. Wang, H. Guo, G. Liu, et al., A triboelectric nanogenerator-based smart insole for multifunctional gait monitoring, Adv. Mater. Technol. 4 (2019) 1800360, https://doi.org/10.1002/admt.201800360.

[25] Y. Wang, X. Yu, M. Yin, J. Wang, Q. Gao, Y. Yu, et al., Gravity triboelectric nanogenerator for the steady harvesting of natural wind energy, Nano Energy 82 (2021) 105740, https://doi.org/10.1016/j.nanoen.2020.105740.

[26] S. Liu, X. Li, Y. Wang, Y. Yang, L. Meng, T. Cheng, et al., Magnetic switch structured triboelectric nanogenerator for continuous and regular harvesting of wind energy, Nano Energy 83(2021), 105851, https://doi.org/10.1016/j.nanoen.2021.105851.

[27] X. Fu, S. Xu, Y. Gao, X. Zhang, G. Liu, H. Zhou, et al., Breeze-wind-energy-powered autonomous wireless anemometer based on rolling contact-electrification, ACS Energy Lett 6 (2021) 2343-2350, https://doi.org/10.1021/acsenergylett.1c00704.

[28] C. Wu, A.C. Wang, W. Ding, H. Guo, Z.L. Wang, Triboelectric nanogenerator: a foundation of the energy for the new era, Adv. Energy Mater. 9 (2019) 1802906, https://doi.org/10.1002/aenm.201802906.

[29] X. Lu, Y. Xu, G. Qiao, Q. Gao, X. Zhang, T. Cheng, et al., Triboelectric nanogenerator for entire stroke energy harvesting with bidirectional gear transmission, Nano Energy 72 (2020) 104726, https://doi.org/10.1016/j.nanoen.2020.104726.

[30] L. Liu, Q. Shi, J.S. Ho, C. Lee, Study of thin film blue energy harvester based on triboelectric nanogenerator and seashore IoT applications, Nano Energy 66 (2019) 104167, https://doi.org/10.1016/j.nanoen.2019.104167.

[31] J. Kolehmainen, P. Sippola, O. Raitanen, A. Ozel, C.M. Boyce, P. Saarenrinne, et al., Effect of humidity on triboelectric charging in a vertically vibrated granular bed: Experiments and modeling, Chem. Eng. Sci. 173 (2017) 363-373, http://dx.doi.org/10.1016/j.ces.2017.08.006.

[32] P.S. Gil, D.J. Lacks, Humidity transforms immobile surface charges into mobile charges during triboelectric charging, Phys. Chem. Chem. Phys. 21(2019) 13821-13825, https://pubmed.ncbi.nlm.nih.gov/31211312/.

[33] A.C. Wang, B. Zhang, C. Xu, H. Zou, Z. Lin, Z.L. Wang, Unraveling Temperature-Dependent Contact Electrification between Sliding-Mode Triboelectric Pairs, Adv. Funct. Mater. 30 (2020) 1909384, https://doi.org/10.1002/adfm.201909384.

[34] C. Xu, A.C. Wang, H. Zou, B. Zhang, C. Zhang, Y. Zi, et al., Raising the Working Temperature of a Triboelectric Nanogenerator by Quenching Down Electron Thermionic Emission in Contact-Electrification, Adv. Mater. 30 (2018) e1803968, https://doi.org/10.1002/adma.201803968.

[35] J. Fu, G. Xu, C. Li, X. Xia, D. Guan, J. Li, et al., Achieving ultrahigh output energy density of triboelectric nanogenerators in high-pressure gas environment, Adv. Sci. 7 (2020) 2001757, http://dx.doi.org/10.1002/advs.202001757.

[36] J. Wang, C. Wu, Y. Dai, Z. Zhao, A. Wang, T. Zhang, et al., Achieving ultrahigh triboelectric charge density for efficient energy harvesting, Nat. Commun. 8 (2017) 88, http://dx.doi.org/10.1038/s41467-017-00131.

[37] J. Chun, J.W. Kim, W.-s. Jung, C.-Y. Kang, S.-W. Kim, Z.L. Wang, et al., Mesoporous pores impregnated with Au nanoparticles as effective dielectrics for enhancing triboelectric nanogenerator performance in harsh environments, Energy Environ. Sci. 8(2015) 3006-3012, http://dx.doi.org/10.1039/C5EE01705J.

[38] J.W. Lee, S. Jung, J. Jo, G.H. Han, D.-M. Lee, J. Oh, et al., Sustainable highly charged C60-functionalized polyimide in a non-contact mode triboelectric nanogenerator, Energy Environ. Sci. 14 (2021) 1004-1015, http://dx.doi.org/10.1039/D0EE03057K.

[39] K.-W. Lim, M. Peddigari, C.H. Park, H.Y. Lee, Y. Min, J.-W. Kim, et al., A high output magneto-mechano-triboelectric generator enabled by accelerated water-soluble nano-bullets for powering a wireless indoor positioning system, Energy Environ. Sci. 12 (2019) 666-674, http://dx.doi.org/10.1039/C8EE03008A.

[40] W. Liu, Z. Wang, G. Wang, Q. Zeng, W. He, L. Liu, et al., Switched-capacitor-convertors based on fractal design for output power management of triboelectric nanogenerator, Nat. Commun. 11 (2020) 1883,| https://doi.org/10.1038/s41467-020-15676-y.

[41] Z. Wang, W. Liu, W. He, H. Guo, L. Long, Y. Xi, et al., Ultrahigh electricity generation from low-frequency mechanical energy by efficient energy management, Joule 5 (2021) 441-55, https://doi.org/10.1016/j.joule.2020.12.023.

[42] F. Xi, Y. Pang, W. Li, T. Jiang, L. Zhang, T. Guo, et al., Universal power management strategy for triboelectric nanogenerator, Nano Energy 37(2017) 168-176, https://doi.org/10.1016/j.nanoen.2017.05.027.

[43] H. Zou, Y. Zhang, L. Guo, P. Wang, X. He, G. Dai, et al., Quantifying the triboelectric series, Nat. Commun., 10 (2019) 1427, 427 | https://doi.org/10.1038/s41467-019-0.

[44] J.W. Peterson, Contact charging between nonconductors and metal, J. APPL. PHYS. 25 (1954) 907-915, http://dx.doi.org/10.1063/1.1721768.

[45] Y. Liu, W. Liu, Z. Wang, W. He, Q. Tang, Y. Xi, et al., Quantifying contact status and the air-breakdown model of charge-excitation triboelectric nanogenerators to maximize charge density, Nat. Commun., 11(2020) 1599, https://doi.org/10.1038/s41467-020-15368-9.

[46] C. Xu, Y. Zi, A.C. Wang, H. Zou, Y. Dai, X. He, et al., On the electron-transfer mechanism in the contact-electrification effect, Adv. Mater. 30 (2018) e1706790, https://doi.org/10.1002/adma.201706790.

Highlights

Highlights and breakthroughs in our research:

1. The mechanism underlying TENG under different mechanical motions is revealed.
2. Two new mechanical motions of TENG are proposed.
3. The mechanism of different mechanical motions on TENG's performance is analyzed.
4. The theoretical models of dynamic charging and discharging are established.

Yang Yu was born in 1995 Jilin province, majored in mechanical engineering, and achieved the B.E. and M.S. degrees from Changchun University of Technology. He is currently pursuing Ph.D. degree in Beijing Institute of Nanoenergy and Nanosystems. His research interest is triboelectric nanogenerator.

Qi Gao was born in 1995 Jilin province, majored in mechanical engineering, and achieved the B.S. and M.S. degree from Changchun University of Technology in 2017 and 2020, respectively. He continues pursuing Ph.D. degree in Beijing Institute of Nanoenergy and Nanosystems. His research interest is triboelectric nanogenerator.

Da Zhao received the M.S. degree from Changchun University of Technology, China, in 2020. He is currently studying for his Ph.D. degree in School of Mechatronic Engineering at Changchun University of Technology, and is also a visiting student in Beijing Institute of Nanoenergy and Nanosystems. His research interests focus on triboelectric nanogenerators and piezoelectric energy harvester.

Xiang Li achieved the B.S. degree from the Shenyang University of Technology in 2018. He is studying for a master's (M.S.) degree in mechanical engineering at Shenyang Jianzhu University. Now, he is a visiting student at Beijing Institute of Nanoenergy and Nanosystems. His research interest is environmental energy harvesting by triboelectric nanogenerators.

Prof. Zhong Lin Wang received his Ph.D. from Arizona State University in physics. He now is the Hightower Chair in Materials Science and Engineering, Regents' Professor, Engineering Distinguished Professor and Director, Center for Nanostructure Characterization, at Georgia Tech. Dr. Wang has made original and innovative contributions to the synthesis, discovery, characterization and understanding of fundamental physical properties of oxide nanobelts and nanowires, as well as applications of nanowires in energy sciences, electronics, optoelectronics and biological science. His discovery and breakthroughs in developing nanogenerators established the principle and technological road map for harvesting mechanical energy from environment and biological systems for powering personal electronics. His research on self-powered nanosystems has inspired the worldwide effort in academia and industry for studying energy for micro-nano-systems, which is now a distinct disciplinary in energy research and future sensor networks. He coined and pioneered the field of piezotronics and piezophototronics by introducing piezoelectric potential gated charge transport process in fabricating new electronic and optoelectronic devices. Details can be found at: http:// www.nanoscience.gatech.edu.

Prof. Tinghai Cheng received the B.S., M.S. and Ph.D. degrees from Harbin Institute of Technology in 2006, 2008 and 2013, respectively. He was a visiting scholar in the School of Materials Science and Engineering at Georgia Institute of Technology from 2017 to 2018. Currently, he is a professor of Beijing Institute of Nanoenergy and Nanosystems, Chinese Academy of Sciences. His research interests are triboelectric nanogenerators, piezoelectric energy harvester, and piezoelectric actuators.

Declaration of interests

☒ The authors declare that they have no known competing financial interests or personal relationships that could have appeared to influence the work reported in this paper.

☐The authors declare the following financial interests/personal relationships which may be considered as potential competing interests: